J Nanostruct 14(2): 392-410, Spring 2024

RESEARCH PAPER

Novel Thiazolyl Azo Dyes: Elucidating the Design, Synthesis, Spectral Characterization, Cytotoxicity, and Antibacterial Potential of its Co(III), Ni(II), and Cu(II) NanoComplexes

*Suha Hassan Majhool *, Azal Shakir Waheeb, Masar Ali Awad*

Department of Chemistry, College of Science, University Al- Muthanna, Iraq

ARTICLE INFO

Article History:
Received 22 January 2024
Accepted 20 March 2024
Published 01 April 2024

Keywords:
Cell line
Characterization
Metals
Nanocomplxes

ABSTRACT

2-[2-(5-Methylethiazolyl) azo] and the combination of its cobalt(III), nickel(II), and copper(II) complexes yields the new bidentate azo dye ligand 5,6-dimethylbenzimidazole (5-MeTADMBI). The suggested structures were found by using atomic absorption spectroscopy, molar conductivity, magnetic susceptibility, nuclear magnetic resonance (^{1}H NMR) and ^{13}C NMR, Fourier transforms infrared (FTIR), ultraviolet-visible (UV-Vis), mass spectrometry, X-ray diffraction (XRD), thermogravimetric analysis (TGA/DTG), and scanning electron microscope field emission (FE-SEM). All complexes have been given geometry suggestions according to analytical and spectroscopic data with cobalt(III), nickel(II), and copper(II) ions, the 5-MeTADMBI ligand takes an octahedral shape via N, N donors and behaves as a bidentate. The biological testing of the synthesized compounds against Escherichia coli, Staphylococcus aureus, Klebsiella and candida. revealed increased antibacterial activity. Their testing revealed that the metal complexes are superior against a variety of bacterial and fungal species. Finally, based on IC50, most of the compounds exhibited potent anticancer activity towards both the A549 human lung cancer cell line and the normal human lung fibroblast HdFn cell line.

How to cite this article
Majhool S H., Waheeb A S., Awad M A. Novel Thiazolyl Azo Dyes: Elucidating the Design, Synthesis, Spectral Characterization, Cytotoxicity, and Antibacterial Potential of its Co(III), Ni(II), and Cu(II) Nano Complexes. J Nanostruct, 2024; 14(2):392-410. DOI: 10.22052/JNS.2024.02.004

INTRODUCTION

Today, azo dyes form the majority of dye chemistry output, and their popularity may grow in the years to come. The synthesis of most azo dyes involves the diazotization of an aromatic primary amine, followed by its subsequent coupling to one or more electron-rich nucleophiles, commonly amino or hydroxyl groups. Azo dyes get their color from the chromophores and auxochromes that bind to their azo bonds. Due to their exceptional biological and physicochemical qualities and wide range of uses in fields as varied as analytical chemistry, pharmaceuticals, cosmetics, painting, and the dyeing industry, azo dyes have garnered considerable interest [1,2].

Extensive investigation has been dedicated to exploring the notable therapeutic properties exhibited by small-ring heterocycles that incorporate N and S atoms [3]. Thiazole and imidazole derivatives are among the most important heterocyclic compounds due to their biological and chemical potential as well as their presence in major classes of naturally occurring compounds (such as alkaloids, vitamins,

* *Corresponding Author Email: suhahassan002@gmail.com*

hormones, and antibiotics). There has been an increase in the usage of imidazoles and thiazoles as organic synthesis intermediates, catalysts for asymmetric synthesis, and active ligands for transition metals and their complexes [4,5]. These chemicals affect DNA by changing its structure, activity, and stability. Due to the suppression of enzymes involved in DNA metabolism, including topoisomerases, several critical cellular processes are disrupted [6]. The biological activities exhibited by thiazole and imidazole are anti-inflammatory [7], antibacterial, antifungal [8], antitumor, anti-tubercular, anti-diabetic, antiviral, and anticancer [9].

More than 10 million people die every year from cancer, which is part of a group of disorders characterized by aberrant cell division and unchecked cell development. The challenge for synthetic chemists is to create anticancer medications that are both more selective and less toxic. In pharmacology, heterocyclic molecules typically play an important function. Thiazoles and imidazoles are just two of the many NN and NS-donating ligands and their metallic complexes that were discovered as anti-cancer agents in the past 35 years [10,11].

This research involved the synthesis of a new thiazolyl azo ligand (5-MeTADMBI) and the evaluation of its antibacterial activity against Gram (-ve, +ve) bacteria using a range of Co(III), Ni(II), and Co(II) complexes [12]. Finally, the chemicals were tested for their anti-cancer activity in a cytotoxicity experiment using Lung cancer (A549) cell lines [13].

MATERIALS AND METHODS

Instruments

Infrared compound spectra were registered using (KBr disc) in the range (400- 4000) cm^{-1} of a Shimadzu 8400S FT-IR spectroscopy. The ^{1}H and ^{13}C NMR spectra were run at 500 MHz employing dimethylsulfoxide (DMSO-d6) as the chosen solvent and tetramethylsilane (TMS) as the designated reference compound, we shall proceed with the utilization of a Brukere 500 Analyzer for our experimental endeavors. The mass spectra were recorded with the aid of the AB Sciex 3200 QTRAP device. The UV-Vis spectra

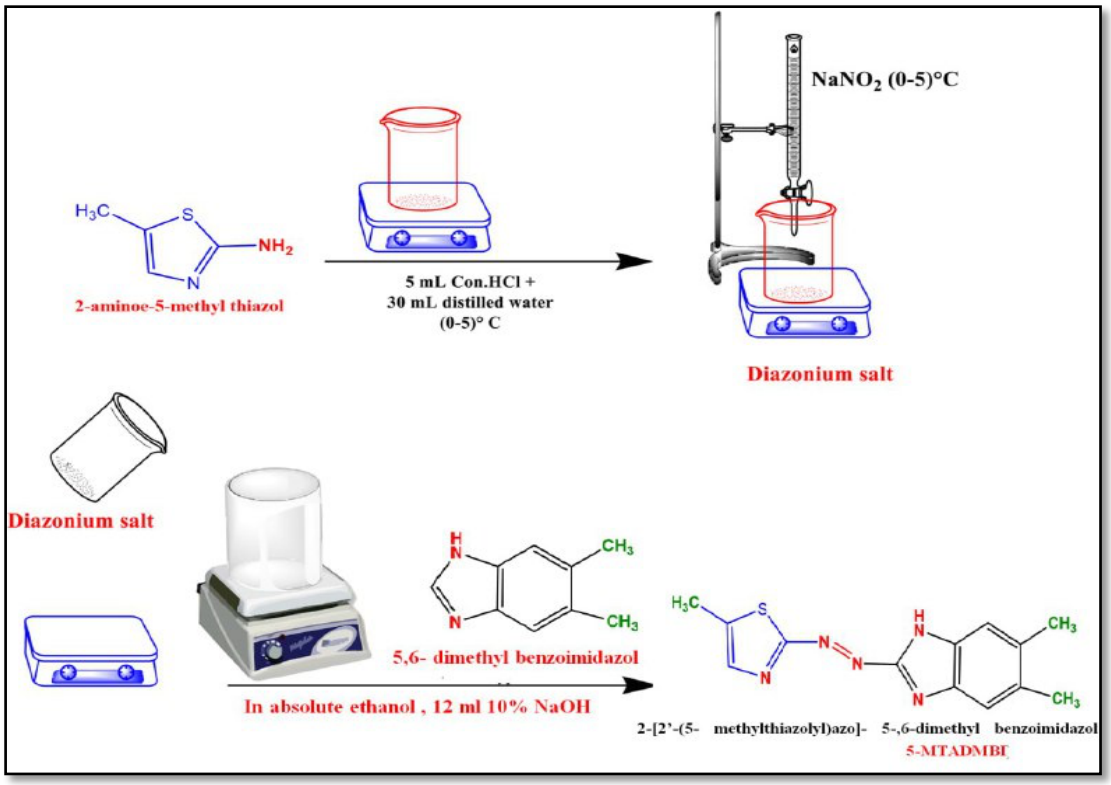

Fig. 1. Synthesis of (5-MeTADMBI) azo ligand

were measured using a PerkinElmer Ultraviolet-Visible Spectrometer Lambda 35. Spectroscopy (C.H.N.) was performed using a Euro EA 1106 elemental analyzer. The BuchiSMP-20 was used to determine the ligand and complex melting points. The magnetic susceptibility of the complexes was tested for each sample using the Susceptibility Balance Magnetic Model M.S.B.-Auto. The X-ray diffraction (XRD) analysis was carried out on a Siemens D5000. The scanning electron microscope technique was used in the emitted field (FESEM TESCAN BRNO-MIRA3 LMU, which is of Czech-French origin). At room temperature (240 °C), ethanol solutions were tested using a 31A digital conductivity meter to determine their conductivity. Perkin-Elmer instruments were utilized to analyze the compounds' thermal stability after synthesis.

Material

All of the substances in this experiment come from commercially available, high-quality sources of analytical reagents. Aldrich, Sigma (Germany), Merck (Germany), and J&K chemical (China) supplied the 2-amino-5- methyl thiazole, 5,6-dimethyl benzimidazole, DMSO (Dimethyl sulfoxide), pure ethanol, $NaNO_2$, NaOH, HCl, $CoCl_2.6H_2O$, and $NiCl_2.6H_2O$.

Synthesis of 2-[2-(5-Methyle thiazolyle) azo]-5, 6-dimethyl benzimidazole (5-MeTADMBI)

Fig. 1 shows the steps taken to synthesize a new thiazolyl azo dye ligand, 2-[2-(5-Methyle thiazolyle) azo]-5, 6-dimethyl benzimidazole (5-MeTADMBI). According to the literature[14,15], we dissolved 2-amino-5-methylthiazole (1.2g, 0.001 moles) in concentrated hydrogen chloride (5 mL) and distilled water (30 mL) to make the diazonium salt. Within 30 minutes of cooling in an ice-water bath with constant stirring, (1g, 0.015 mol.) of $NaNO_2$ dissolved in, (35 mL) of deionized water was applied. However, after stirring the reaction mixture in an ice bath (0-5 °C) for an hour, a solution of (diazonium salt) was slowly added to a solution of 5,6-dimethyl benzo imidazole (1.5g, 0.01 mole) dissolved in the mixture (25 mL Ethyl alcohol, 12 mL 10% NaOH). The precipitate was obtained after filtering and cooling. Several washes in distilled water, a recrystallization in Ethyl alcohol, and an overnight drying at 50 °C resulted in a pure precipitate.

General synthesis of metal complexes

To produce metal complexes, ligand (0.3g, 0.002 moles) was dissolved in ethanol solution (50 mL). In a stoichiometric ratio of 1:2 [M: L] for $Co^{(III)}$ and $Cu^{(II)}$ and 1:1 [M: L] for $Ni^{(II)}$, add (0.15g, 0.0001 moles) of metal chlorides while stirring and utilize the buffer solution (ammonium acetate). Over 30 minutes at (50-70°C) and left overnight, the reaction mixture was gradually lowered. Several methods were used to re-crystallize the solid metal complexes after washing them in a distilled water/ ethanol solution and drying them Table 1 [16].

RESULTS AND DISCUSSION

Characterization of thiazolyl azo dye ligand and their complexes

Brown crystals of the novel (5-MeTADMBI) ligand were seen, while crystals of the synthesized metallic complexes appeared to be of varied colors. The compounds exhibit limited solubility in aqueous media while demonstrating appreciable solubility in organic solvents such as ethanol, DMSO-d_6, or methanol [17,18]. All of the compounds are stable at ambient temperature. Thiazolyl azo ligand and chelate complex yields, melting temperatures, and elemental analyses are shown in Table 1.

Molar conductivity and stability constants measurements

Table 2 shows that all of the metal complexes are not an electrolyte in a 10^{-3} Molarity ethanol solution at ambient temperature, however,

Table 1. Ligand (5-MeTADMBI) and metal complex physicochemical characteristics.

Compound	Color	m.p°c	λ_{max} (nm)	Yield%	Molecular Formula (M.wt) (g/mol)	Mole ratio [M:L]
5-MeTADMBI	Brown	128 °C	458	85	$C_{13}H_{13}N_5S$ 271.34	---
$[Co(L)_2Cl_2]Cl.H_2O$	Bluish - green	231 °C	629	79	$C_{26}H_{28}N_{10}S_2OCoCl_3$ 726.003	1:2
$[Ni(L)_1Cl_2].H_2O$	Olive green	138 °C	585	83	$C_{13}H_{15}N_5SONiCl_2$ 418.962	1:1
$[Cu(L)_2Cl_2].H_2O$	Dark green	227 °C	637	72	$C_{26}H_{28}N_{10}S_2OCuCl_2$ 695.263	1:2

Table 2. Maximum wavelength (λ_{max}), best concentration, molar conductivity, and stability constants values (β and Log β) of metal complexes.

Metal Ions Complex	(λ_{max})nm	Best Conc.×10^{-4} M	β	Log β	Molar conductivity S.cm^2. mol^{-1}
Co(III)	629	1.75	4.75×10^9	9.67	37.46
Ni(II)	585	1.5	1.54×10^8	8.18	10.22
Cu(II)	637	2.00	1.76×10^9	9.24	12.73

based on its conductivity, the Co(III)-complex is an electrolyte[19,20]. Furthermore, the determination of stability constants for all complexes entails the utilization of absorbance coefficients obtained from solutions comprising both ligand and metal ions at a fixed wavelength (λmax). In relation to the equations:

$$\beta = (1\text{-}\alpha)/4\ \alpha^3C^2,\ [1{:}2]\ [M{:}\ L]$$

$$\beta = (1\text{-}\alpha)/\ \alpha^2C,\ [1{:}1]\ [M{:}\ L]$$

$$\alpha = \text{Am-As/Am}$$

Where As and Am are the Absorbance of fully and partially produced metallic complexes at best concentrations, respectively [21,22].

UV-Vis Studies

In order to elucidate the stereochemistry or geometry of metal complexes, it is imperative to consider two key parameters: the maximum wavelength of electronic absorption (λ_{max}, nm) and the magnetic moment (μ_{eff} B.M.) at room temperature. The UV-Vis spectra of a 10^{-4} M solution of the free ligand (5-MTADMBI) and its complexes in absolute ethanol at ambient temperature within the wavelength range of 200 to 1100 nm are depicted in both Fig. 2 and Table 3 [23].

The electronic spectrum of a free ligand (5-MTADMBI) showed four absorption peaks, the first at wavelength 458nm (21834.06)cm^{-1} belonging to an electron transition (n→π(* of an azo group -)N=N(- and the second at wavelength 398nm (25125.63)cm^{-1} belonging to the electron transition (n→π (*of an)C=N (imine group in the thiazole ring, as well as, a third peak appeared at 326nm (30674.85 cm^{-1}) and the fourth peak at 270nm (37037.04 cm^{-1}) is related to the electronic transition (π→π (*of the)C=C(bond in the thiazole ring and the aromatic ring [24,25].

Three absorption peaks were observed in the UV spectrum of the $Co^{(III)}$-Complex at 629nm (15898.25 cm^{-1}), 319nm (31347.96 cm^{-1}), and 266nm (37593.98 cm^{-1}) due to $^1A_1g \rightarrow {}^1T_2g_{(F)(\upsilon 1)}$, $^1A_1g \rightarrow {}^1T_1g_{(F)(\upsilon 2)}$, and $^1A_1g \rightarrow {}^1T_1g_{(p)(\upsilon 3)}$, and other peaks returning to the transitions of the intra ligand. Transitions

Table 3. Electronic spectra, magntic moment, geomeitry and hybridezation of the (5-MTADMBI) ligand and metalic complexes.

Compounds	λ_{max} (nm)	Absorption Bands (cm^{-1})	Transitions	μ_{eff} (B.M)	Geometry	Hybridization
LH = (5-MTADMBI)	458	21834.06	n →π*	-	-	-
	398	25125.63	*n →π			
	326	30674.85	π →π*			
Co(III) Complex	270	37037.04	π →π*	Dia	Octahedral (Regular)	d^2sp^3 Low spin
	629	15898.25	$^1A_1g \rightarrow {}^1T_2g_{(F)(\upsilon 1)}$			
	319	31347.96	$^1A_1g \rightarrow {}^1T_1g_{(F)(\upsilon 2)}$			
	266	37593.98	$^1A_1g \rightarrow {}^1T_1g_{(p)(\upsilon 3)}$			
	430	23255.81	Intra ligand			
Ni(II) Complex	505	19801.98	$^1A_1g \rightarrow {}^1A_2g_{(\upsilon 1)}$	Dia	Square planer	dsp^2
	325	30769.23	$^1A_1g \rightarrow {}^1B_1g_{(\upsilon 2)}$			
	269	37174.72	$^1A_1g \rightarrow {}^1Eg_{(\upsilon 3)}$			
	420	23809.52	Intra ligand			
Cu(II) Complex	637	15698.59	$^2B_1g \rightarrow {}^2A_1g$ $_{(dx2\text{-}y2 \rightarrow dz2)}$ $(\upsilon 1)$ $^2B_1g \rightarrow {}^2B_2g$ $_{(dx2\text{-}y2 \rightarrow dyz)}$ $(\upsilon 2)$ $^2B_1g \rightarrow {}^2B_2g$ $_{(\text{charge transfer})}(\upsilon 3)$	1.746	Octahedral (Distorted) (Z-in or Z-out)	Sp^3d^2 Low spin
	427	23419.20	Intra ligand			
	292	34246.58	Intra ligand			

with an octahedral geometry have been measured to have a magnitude of 10Dq/B (34.5) using the ratio υ_2/υ_1 (1.73). For the octahedral structure, we can use the tanaba-Sugano diagram for the d^6 structure, the magnitude of B' (565) as well as a location of υ_1(10Dq) (12447.36) cm^{-1} have been examined. The value of β (0.514) denotes some covalent character. According to the conductivity test done with ethanol as the solvent, the Co(III)-Complex is an electrolyte[26][27].

The electronic spectrum of the $Ni^{(II)}$-complex gave four absorption peaks, three of them at 505 nm (19801.98 cm^{-1}), 325 nm (30769.23 cm^{-1}), and 269 nm (37174.72 cm^{-1}) due to the electron transitions $^1A_1g \rightarrow {}^1A_2g_{(\upsilon 1)}$ and $^1A_1g \rightarrow {}^1B_1g_{(\upsilon 2)}$ and $^1A_1g \rightarrow {}^1Eg_{(\upsilon 3)}$ respectively, while the other transition at 420 nm (23809.52) cm^{-1} is related to the intra ligand, respectively, of square planar geometry [28].

The spectrum of the $Cu^{(II)}$-complex showed a wide absorption peak of moderate intensity at 637nm (15698.59 cm^{-1}), and the reason for the width of the peak indicates the occurrence of three electronic transitions of similar energy, which are $^2B_1g \rightarrow {}^2A_1g_{(dx2\text{-}y2 \rightarrow dz2)(\upsilon 1)}$ and $^2B_1g \rightarrow {}^2B_2g_{(dx2\text{-}y2 \rightarrow dyz)(\upsilon 2)}$ and $^2B_1g \rightarrow {}^2B_2g_{(\text{charge transfer})(\upsilon 3)}$. The reason for the width of the peak in the octahedral field being divided into three peaks is due to the distortion that occurs for this type of complex due to the Jean Teller effect. As for the other absorption peaks at 427nm (23419.20 cm^{-1}) and 292nm (34246.58 cm^{-1}), they are due to intra-ligand transitions. The non-ionic complex conclusion from conductivity measurements [29,30].

C.H.N.S Elemental Analysis

A thorough elemental analysis was conducted employing a CHNS elemental analyzer to elucidate the intricate metallic chemical composition. The elemental analysis yields valuable insights regarding the relative abundances of carbon, hydrogen, nitrogen, and sulfur (CHNS) elements within the material. The precise results of the elemental analysis are meticulously displayed in Table 4.

Upon comparing the experimental and theoretical values, a remarkable degree of concordance was observed, indicating a high level of agreement between the two sets of data. The obtained experimental data provide compelling support for the validity of the selected molar ratios between the metal and ligand species

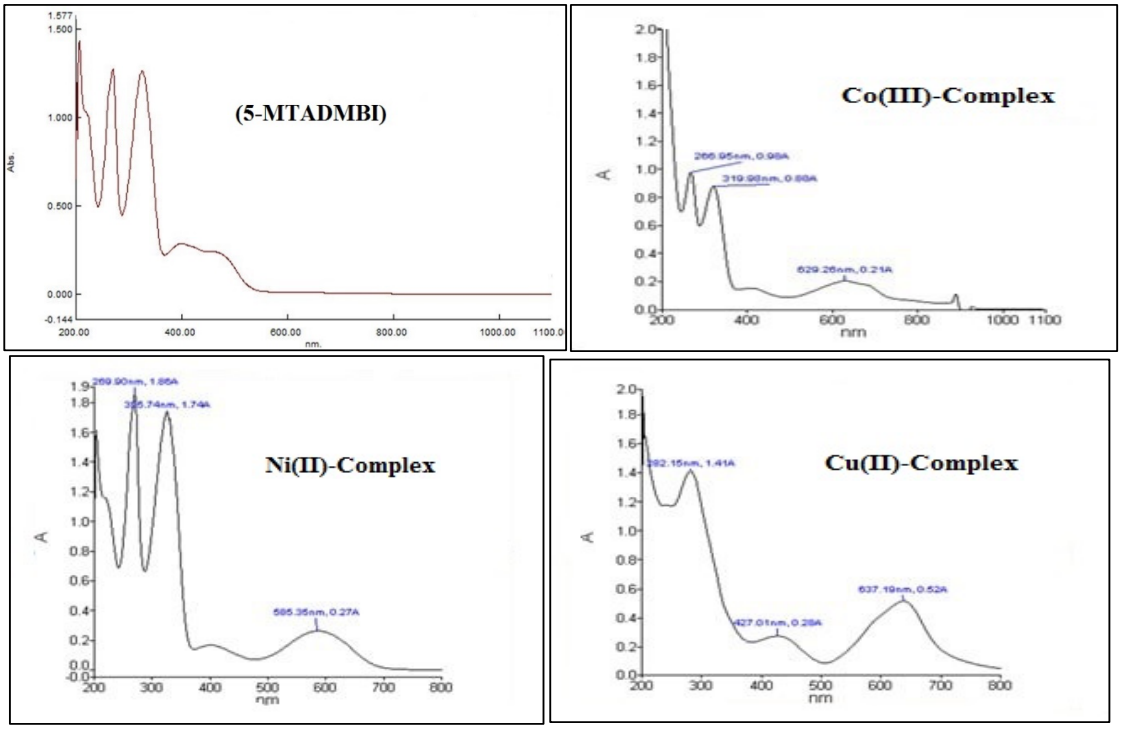

Fig. 2. UV-Vis spectrum of 5-MTADMBI and its metal complexes.

Table 4. The (C.H.N.S) element analysis of the ligand (5-MeTADMBI) and its metal complexes

Compound	Yield%	Molecular Formula (M.wt) (g/mol)	Found% (Calculated)					Mole ratio [M:L]
			C%	H%	%N	%S	%M	
LH = (5-MeTADMBI)	85	)($C_{13}H_{15}N_5S$ 271.34	57.54 (56.12)	5.53) (4.83	25.81 (24.62)	11.82 (10.73)	-	-
$[Co(L)_2Cl_2]Cl.H_2O$	79	$C_{26}H_{28}N_{10}S_2OCoCl_3$ 726.003	44.91 (43.01)	4.05 (3.89)	20.14 (19.29)	9.22 (8.83)	(8.12)	1:2
$[Ni(L)_1Cl_2].H_2O$	83	$C_{13}H_{15}N_5SONiCl_2$ 418.962	37.27 (36.26)	3.61 (2.60)	16.72 (15.71)	7.65 (6.67)	(14.01)	:11
$[Cu(L)_2Cl_2].H_2O$	72	$C_{26}H_{28}N_{10}S_2OCuCl_2$ 695.263	44.92 (43.95)	4.06 (3.44)	20.15 (19.22)	9.23 (8.55)	(9.14)	1:2

[M: L], thereby bolstering the robustness of the proposed chemical formulas for the synthesized metal complexes [31,32]

^{1}H-NMR studies

The investigation involved the analysis of the (5-MTADMBI) ligand and Co(III) complex's ^{1}H-NMR spectrum at ambient temperature. A (Bruker 500 MHz) spectrometer was employed for this purpose, with DMSO-d_6 serving as the solvent. The reference sample utilized was TMS [33]. The presence of a resonance peak at a chemical shift of (11.73) ppm can be attributed to the protons associated with the (NH) imidazole moiety within the free ligand, specifically 5-MTADMBI. Additionally, the occurrence of a signal at a chemical shift of δ = 7.95 ppm can be attributed to the proton within the thiazole ring. The aromatic protons in the benzimidazole ring of the (5-MTADMBI) compound exhibit a signal at a chemical shift range of δ= (6.90 - 7.24) ppm. On the other hand, the protons in the methyl groups (C-(CH3)) of the thiazole and benzimidazole rings display signals at chemical shifts of δ = (2.37 and 2.19) ppm, respectively. The proton resonance is observed at a chemical shift of δ = (2.39-2.41) ppm, indicating a singlet signal in the presence of the solvent. This information is referenced from source [34]. The ^{1}H-NMR spectrum of the thiazolyl azo ligand (5-MTADMBI) is depicted in Fig. 3.

In the ^{1}H- NMR spectrum of the $Co^{(III)}$-complex, the methyl group (C-(CH3)) on the thiazole ring generates a signal at δ = (2.01- 2.06) ppm, while the $(C-(CH_3)_2)$ on the benzimidazole ring provides a signal at δ = (1.75- 1.93) ppm. The NH group produces a signal at δ = 11.23 ppm (imidazole proton), while the proton in the thiazole ring generates a signal at δ = (7.06 - 7.31) ppm, and

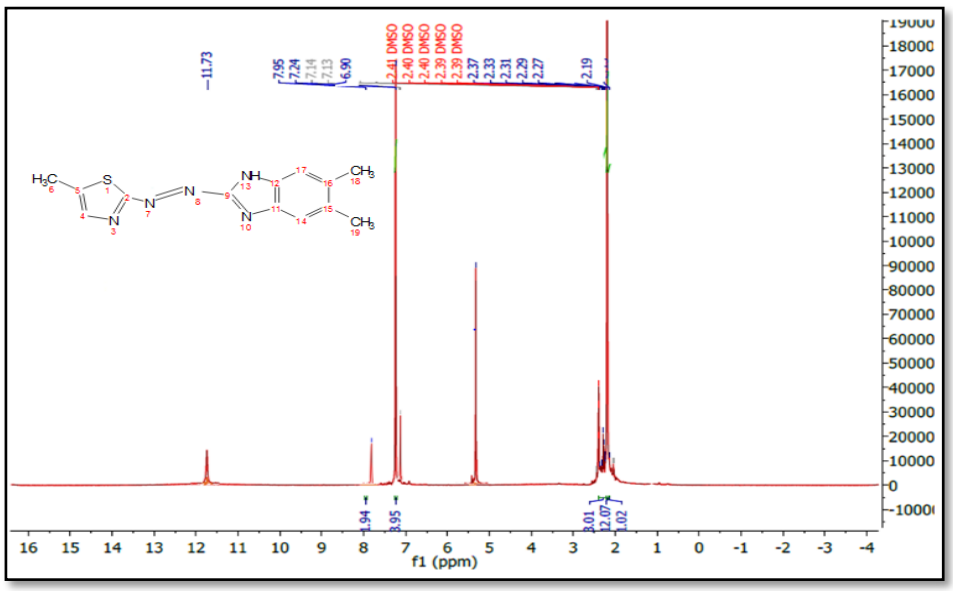

Fig. 3. (5-MTADMBI) ligand ^{1}H-NMR spectra.

the aromatic protons in the benzimidazole ring provide a signal at = (5.20 - 6.63). In the case of the solvent proton shown at = (2.39 - 3.85) ppm [35]. Fig. 4 shows the ^{1}H-NMR spectrum of the Co(III)-complex.

^{13}C-NMR studies

It is possible to determine the type and number of carbon atoms in a molecule by employing ^{13}C-NMR, which is one form of nuclear magnetic resonance technology. Table 5 and Figs. 5 and 6 display the results of ^{13}C-NMR (76 MHz, DMSO-d6) spectra performed on the investigated (5-MTADMBI); these spectra revealed numerous signals at the chemical shifts ^{13}C-NMR= (179.27, 161.76, 156.01, 152.66, 150.57, 143.45, 125.52,

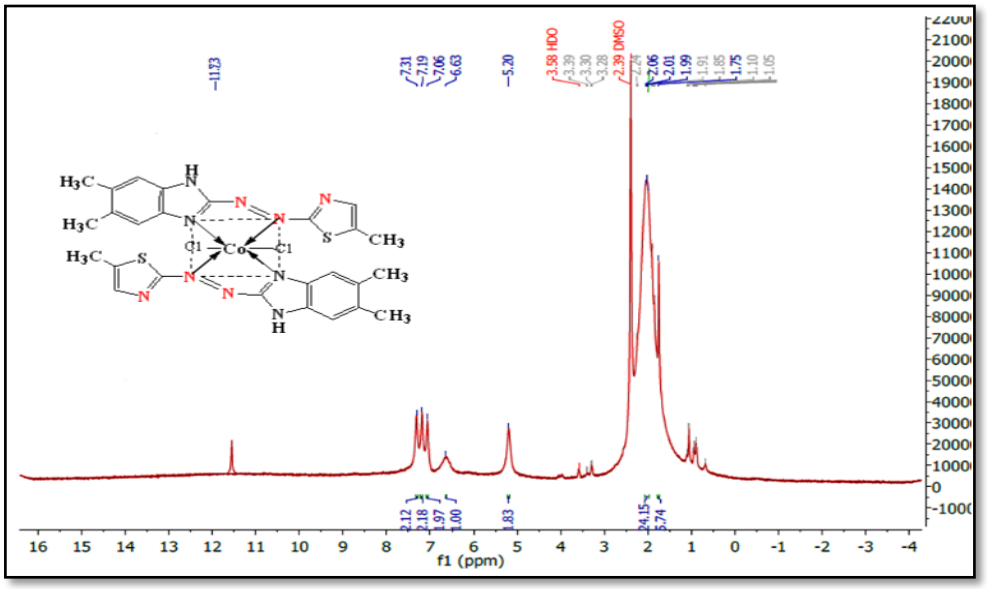

Fig. 4. Cobalt(III)-complex ^{1}H-NMR spectra.

Table 5. Thiazolyl azo ligand and Co(II)-complex ^{13}C-NMR spectra.

LH = 5-MTADMBI		Co(III)-Complex	
Chemical Shiift (ppm)	Position	Chemical Shiift (ppm)	Position
179.27	C_2	170.80	C_2
161.76	C_{12}	161.79	C_{12}
156.01	C_{16}	156.06	C_{16}
152.66	C_4	150.49	C_4
150.57	C_{15}	149.93	C_{15}
143.45	C_5	140.37	C_5
125.52	C_{17}	125.55	C_{17}
123.54	C_{14}	117.79	C_{14}
55.44	C_9	40.41	C_9
26.65	C_{11}	26.66	C_{11}
16.06	C_{18}	16.07	C_{18}
14.71	C_{19}	14.43	C_{19}
14.42	C_6	11.65	C_6

123.54, 55.44, 26.65, 16.06, 14.71, 14.42, and 39.39 ppm) to the carbon atoms at the locations (C_2, C_{12}, C_{16}, C_4, C_{15}, C_5, C_{17}, C_{14}, C_9, C_{11}, C_{18}, C_{19}, C_6, and C solvent) respectively. Signals at δ= (170.80, 161.79, 156.06, 150.49, 149.93, 140.37, 125.55, 117.79, 40.41, 26.66, 16.07, 14.43, 11.65, and 39.39 ppm) were assigned by chemical shift to carbon atoms in the identical thiazolyl azo ligand positions in the Co-complex spectrum [36,37].

FT-IR spectra studies

Upon conducting a comparative analysis between the FTIR spectra of the ligand and its corresponding metal complexes, notable

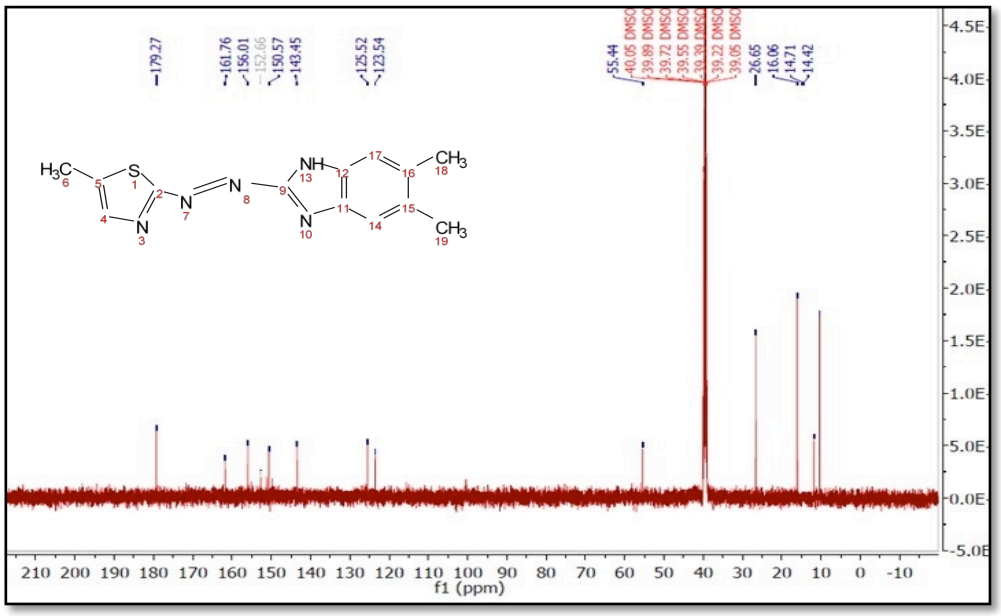

Fig. 5. (5-MTADMBI) ligand ^{13}C-NMR spectra.

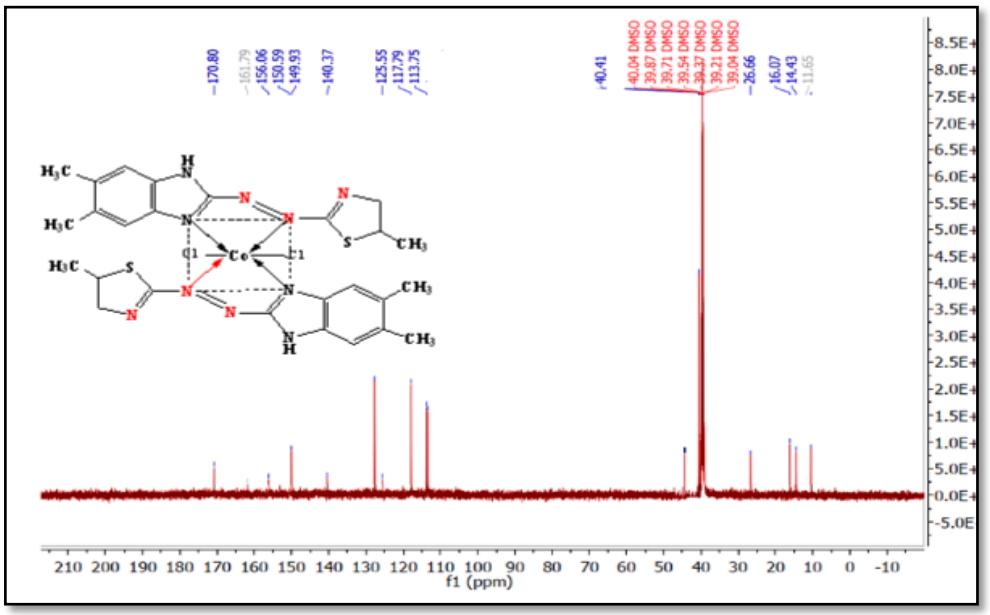

Fig. 6. Co(III)-Complex ^{13}C-NMR spectra.

Table 6. FT-IR spectra of the (5-MTADMBI) ligand and its metal complexes

Group	LH = 5-MTADMBI	Co(III)-Complex	Ni(II)-Complex	Cu(II)-Complex
$\upsilon(H_2O)$	-	3212 s.br.	3363 s.br.	3335 s.br.
$\upsilon(NH)_{Benzimidazole}$	3095 .w	3124 s.br	3203 s.br.	3134 s.br.
$\upsilon(CH)_{Aromatic}$	3030 .m.br.	2970 m.	2974 m.	3080 s.br
$\upsilon(CH)_{Aliphatic}$	2962 .m.br.	2939 m.	2939 m.	2978 s.br.
$\upsilon(C=N)_{Benzimidazole}$	1708 w.	-	-	-
$\upsilon(C=N)_{Thiazole}$	1614 .m	1610 m.br.	1612 m.	1612 m.
υ(N=N)	1477 s.	1498 s.	1502 m.	1498 s.
υ(C=C)	1305 s.	1307 m.	1307 w.	1307 w.
υ(C-S)	1271 s.	1263 s.	1267 m.	1265 m.
υ(C-N)	1159 m.	1203 m.	1203 m.	1207 m.
υ(C-C)	1026 m.	1085 w.	1147 w.	1082 w.
υ (M-N)	-	854 w.	860 m.	773 s.

S = strong, m = medium, w = weak, br = broad, sh = sharp, * = (H2O) outside of sphere coordination.

observations were made. Specifically, certain bands exhibited shifts in their positions, while novel bands emerged, alongside the persistence of unchanged bands. This observation provides evidence for the formation of a chemical complex. The FTIR spectroscopic data pertaining to the (5-MeTADMBI) ligand, along with its corresponding metal complexes, have been comprehensively presented in Table 6 and visually depicted in Fig. 7. Through the utilization of potassium bromide (KBr), the vibrational frequencies of the predominant molecular entities were observed within the spectral region spanning from 400 to 4000 cm^{-1} [38].

The observed strong absorption broad bands in the region of (3095, 3124, 3203, and 3134) cm^{-1} in all the ligand (5-MTADMBI) and its complexes with Co(III), Ni(II), Cu(II) can be ascribed to the stretching vibrations of the (NH) groups. The suggestion has been made that the spectra of most Co(III), Ni(II), and Cu(II) complexes exhibit the presence of (OH)aqua. This inference is based on the observation of significantly broad absorption bands at (3212, 3363, and 3335) cm^{-1}, as well as the notable absence of this band in the spectra of the unbound ligand [39,40].

The spectra of the (5-MeTADMBI) ligand and its complexes exhibited a medium-broad band in the range of (3030, 2970, 2974, and 3080) cm^{-1}, which can be attributed to the (C-H) aromatic vibrations. Additionally, the bands observed at (2962, 2939, 2939, and 2978) cm^{-1} can be assigned to the (C-H) aliphatic vibrations, respectively [41]. In the spectra of the free ligand and its metal complexes, we observed supplementary bands at wavenumbers 1477, 1498, 1502, and 1498 cm-1. These bands can be attributed to the stretching modes (N=N) of the azo group. Additionally, the band at 1708 cm-1 in the spectrum of (5-MeTADMBI) corresponds to the C=N stretching mode of the azomethine group in the benzimidazole ring, providing evidence for the existence of the ligand. The observed spectral band corresponding to the complexes exhibited an absence in comparison to the spectral band observed for the ligand. The FTIR spectra of the metal complex manifest novel bands that can be attributed to the vibrational mode of the metal-nitrogen azo (ν(M-Nazo)), as documented in Table 6. The FT-IR spectra obtained for the metal complexes indicate that (5-MeTADMBI) exhibits the capability to function as a bidentate ligand, specifically binding to nitrogen atoms from both the (N=N) and (C=N) positions of benzimidazole. This binding arrangement results in the formation of a hexagonal structure [42,43].

X-Ray Diffraction (XRD) studies

X-ray diffraction was used to investigate the crystal structures of the ligand (5-MeTADMBI) and its complexes in their solid states. The analysis was conducted within the angular range of (10-80°) 2θ to elucidate structural properties, including the crystalline structure and crystal size Fig. 8. Micro strains and dislocation density were determined as

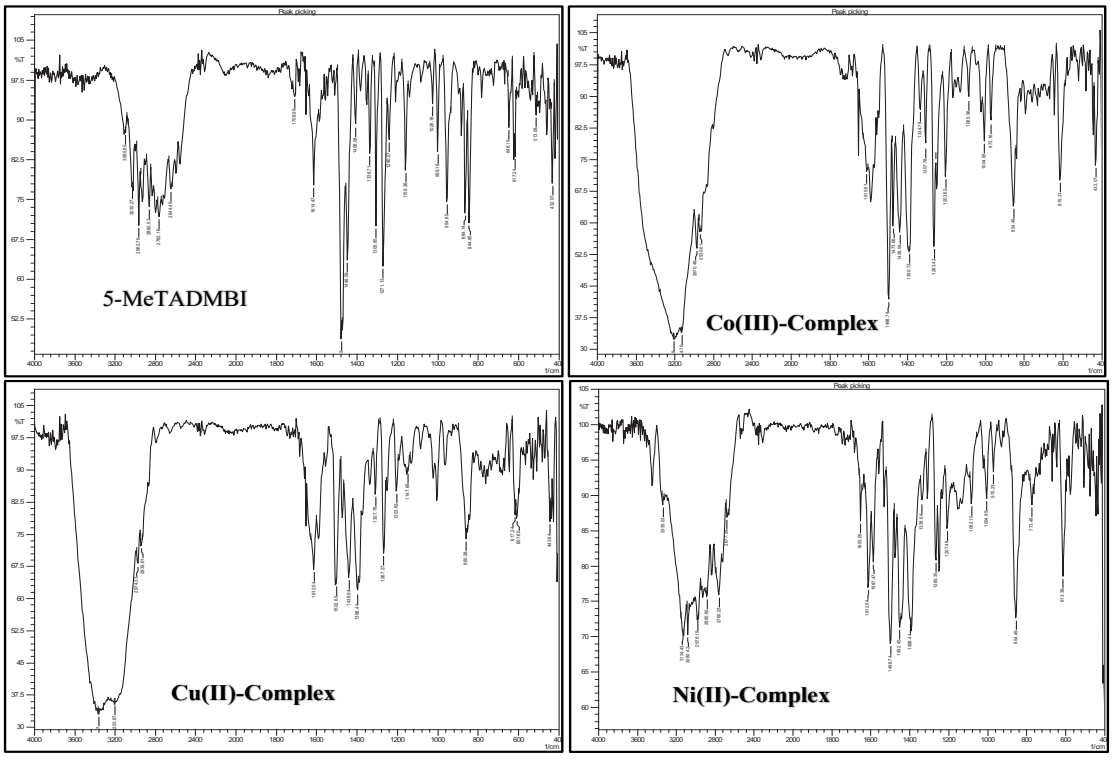

Fig. 7. FTIR spectrum of the (5-MeTADMBI) and its metal complexes.

well to identify the degree of purity and crystalline structure defects during the conversion of the studied ligand into metal complexes [44].

The utilization of Bragg's law [n λ = 2dsin Θ]

Table 7. Crystallographic data of the (5-MeTADMBI) ligand and its complexes.

Ligand	Pos. [°2Th.]	FWHM [°2Th.]	I/I° %	Crystallite Size D (nm)	Lattice strain	d-spacing [A°]	Dislocation density $\delta*10^{-3}$ (nm)^2
1	23.7988	0.3444	100	24.63	0.0071	3.74351	0.0016
2	15.6850	0.2460	54	34.06	0.0078	5.64993	0.8620
3	14.3052	0.4920	38.16	17	0.0171	6.19165	0.0034
4	22.6496	0.3936	33	21.50	0.0086	3.92593	0.0021
Co(L_1)							
1	16.1040	0.1476	100	56.8	0.0046	5.50386	0.3099
2	32.6426	0.3936	51.19	21.98	0.0059	2.74332	0.0020
3	35.68840	0.1968	32.76	44.31	0.0027	2.51587	0.5093
4	21.0312	0.5904	23.21	14.3	0.0139	4.22423	0.0048
5	26.4505	0.1968	18.95	43.33	0.0037	3.36978	0.5326
Ni(L_1)							
1	16.260	0.175	100	47.92	0.0053	5.44695	0.4354
2	22.049	0.11	86.86	76.88	0.0025	4.02813	0.1691
3	34.05	0.19	79.42	45.69	0.0027	2.63094	0.4790
4	28.930	0.16	51.17	53.58	0.0027	3.08382	0.3483
5	26.724	0.12	39.29	71.1	0.0022	3.33310	0.1978
Cu(L_1)							
1	10.203	0.071	100.00	117.39	0.0035	8.66250	0.0725
2	20.783	0.111	95.08	76.03	0.0026	4.27058	0.1729
3	17.994	0.24	76.33	35.01	0.0066	4.92573	0.8158
4	26.040	0.26	60.73	32.76	0.0049	3.41907	0.9317
5	24.657	0.26	47.43	32.68	0.0052	3.60770	0.9363

facilitated the determination of the d-spacing, denoting the separation between the crystalline planes. In this context, n assumes integer values (1, 2, 3, 4), λ corresponds to the wavelength of X-ray Cu-kα (1.5405), and Θ signifies the deflection angle [45]. The Debye-Scherer equation, a fundamental tool in crystallography, allows for the determination of the average crystal size (D) through the utilization of various parameters. In this equation, D is calculated by dividing the product of the X-ray wavelength (λ) and the constant k (known as Blanks constant, with a value of 0.940) by the cosine of the deflection angle (Θ) and the FWHM of a peak observed during experimentation [46]. The ligand and metallic complexes being investigated exhibit a granular size below 100 nm, thereby placing them within the nanoscale regime. Simultaneously, these findings substantiate our previous data obtained through FESEM. Table 7 presents the pertinent data regarding the crystalline size, d-spacing, and diffraction angles pertaining to the synthesized ligand and complexes.

FESEM studies

Using a technique called field emission scanning electron microscopy (FE-SEM), the surface morphology, shape, and aggregation of the particles, as well as their location, of ligand (5-MeTADMBI) and metal complexes are studied. Before imaging, a 20 Kv acceleration voltage, 200 nm cross-sectional distance, and 10 KX magnification force were used with a field emission scanning electron microscope. Fig. 9 displays FESEM images of the thiazolyl azo ligand (LH) and its metal complexes, for which the particle sizes and specific properties were calculated using the (image J) program [47].

The image of the FE-SEM analysis of the (5-MeTADMBI) ligand shows that it has a

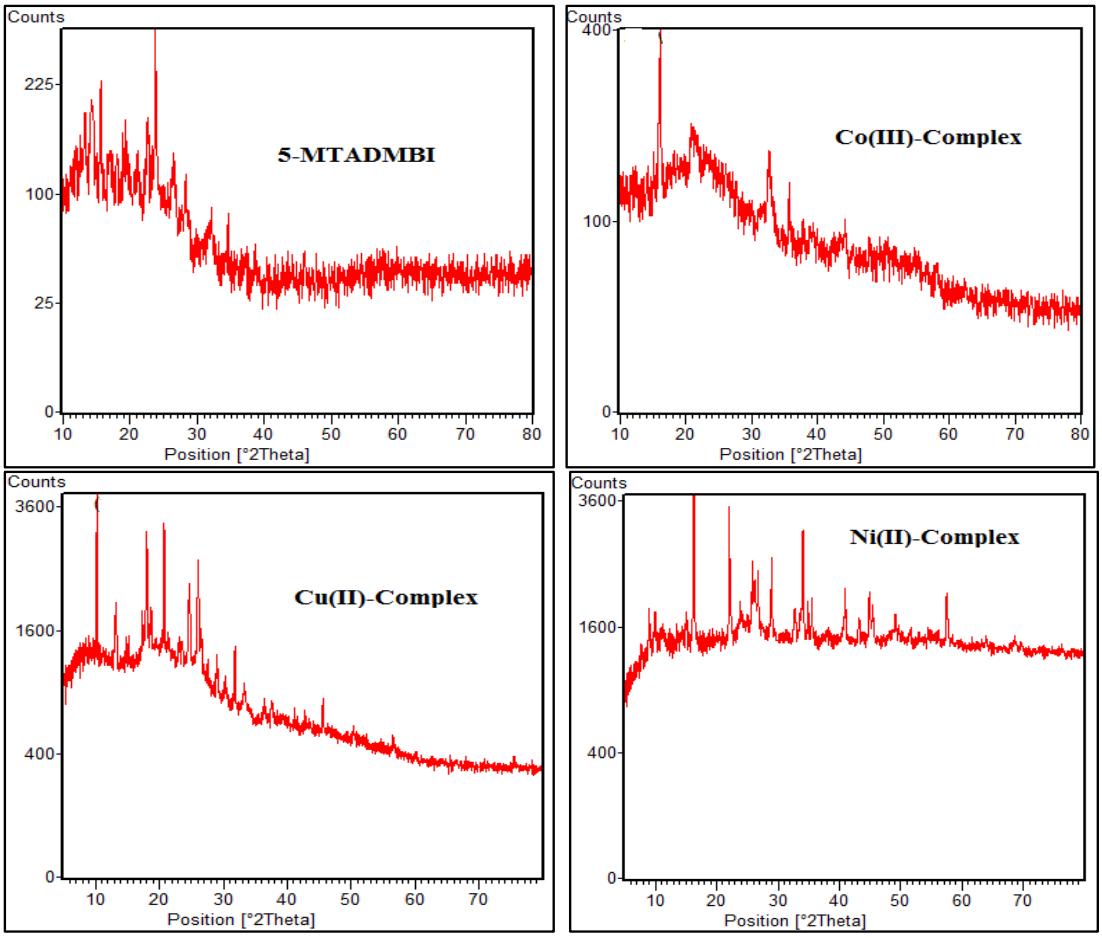

Fig. 8. XRD spectrum of the (5-MeTADMBI) and its metal complexes.

shape with irregular crystalline particles with a heterogeneous surface and an average particle size of (77.42 nm). As for the image of the FESEM analysis of the Co(III)-complex, it appeared in the form of spherical aggregates with an average particle size of (73.63nm). While the image of the FESEM analysis of the Ni(II)-complex showed it in the form of particles, it had a smooth surface with an average particle size of (85.51nm). While the image of the FESEM analysis of the Cu(II)-complex appeared in the form of porous cheese slices and had an average particle size of (66.88nm) [48].

TGA-DTG analysis

The azo dye ligand and its metal complexes underwent thermal treatment in a controlled nitrogen environment, with the temperature ranging from 40 to 900 °C at a heating rate of 20 °C per minute. An experimental investigation utilizing thermogravimetric analysis (TGA) was undertaken with the primary aim of elucidating the thermolytic degradation pathways of the compounds under investigation. Fig. 10 presents the TGA outcomes for the ligand and metal complexes. The TGA data unambiguously demonstrated the occurrence of ligand and complex decomposition in singular, binary, or ternary steps [49].

The thermogravimetric curve for (5-MeTADMBI) one characterization step of decomposition, was seen at temperatures between (40.17 and 410.98°C), and is related to the evolution of moisture and CO2 gas with a loss of mass of 76.095%. There are two successive thermal decomposition stages in the Co(III), Ni(II), and Cu(II), complexes. The initial stage takes place between (39.99- 282.75°C), (40.24 -242.29°C), and (40.36 - 175.17°C) respectively, and it is estimated that (13.536, 16.117, and 5.967 %) of the mass is lost during this stage. A mass loss of about (33.213, 39.381, and 42.263 %) is anticipated to occur during the second stage, which takes place between (258.28- 499.16°C), (242.29 -500.66°C),

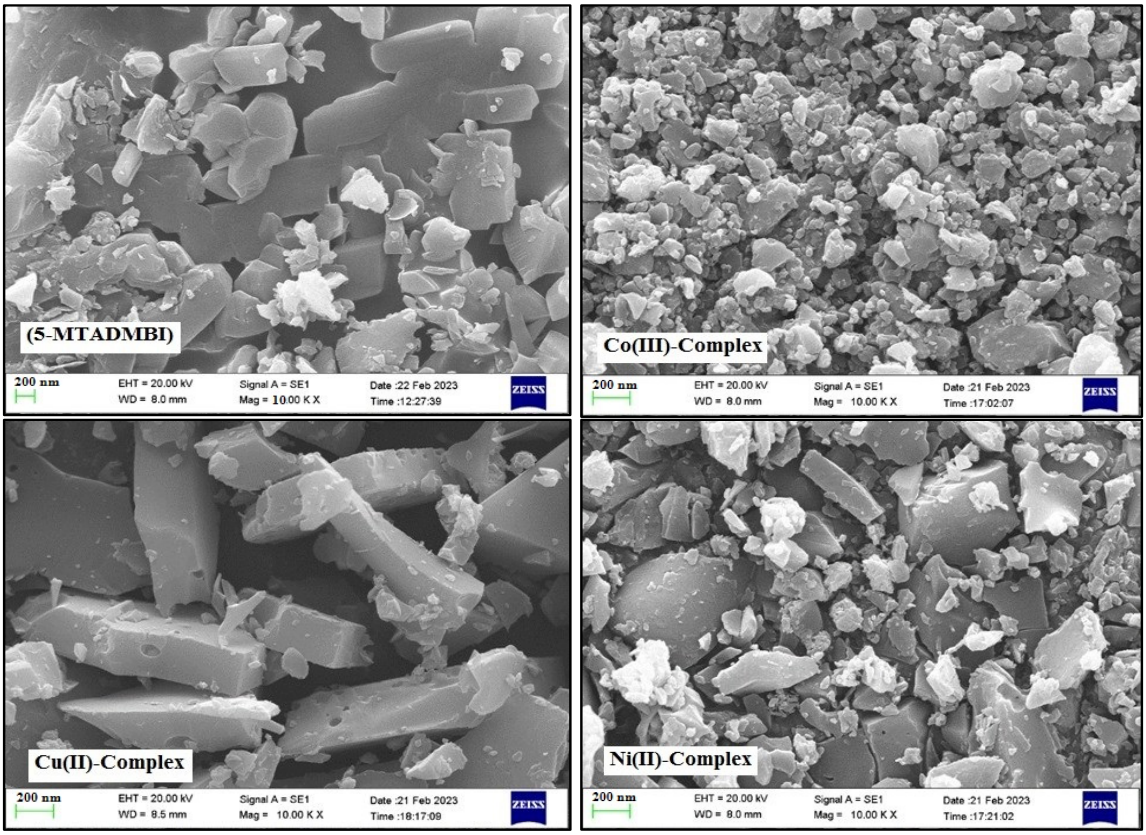

Fig. 9. (5-MTADMBI) ligand and metal complexes FE-SEM images

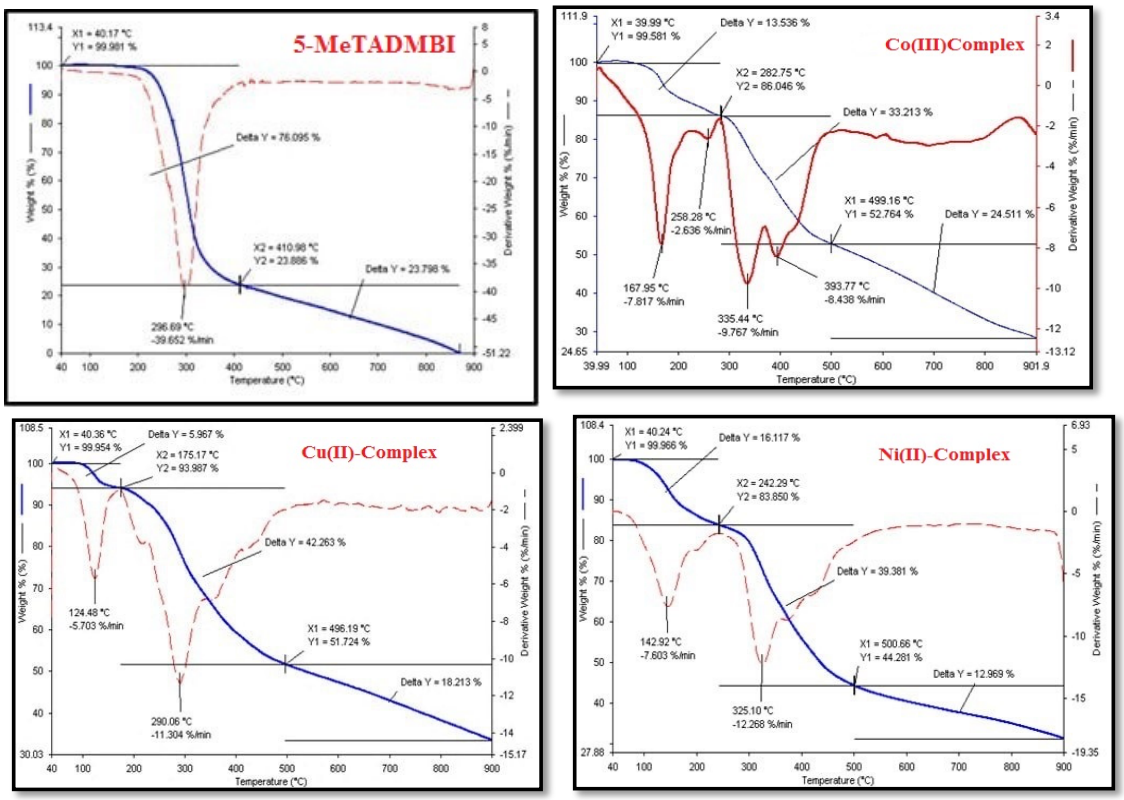

Fig. 10. TGA-DTG analysis for (5-MeTADMBI) ligand and complexes.

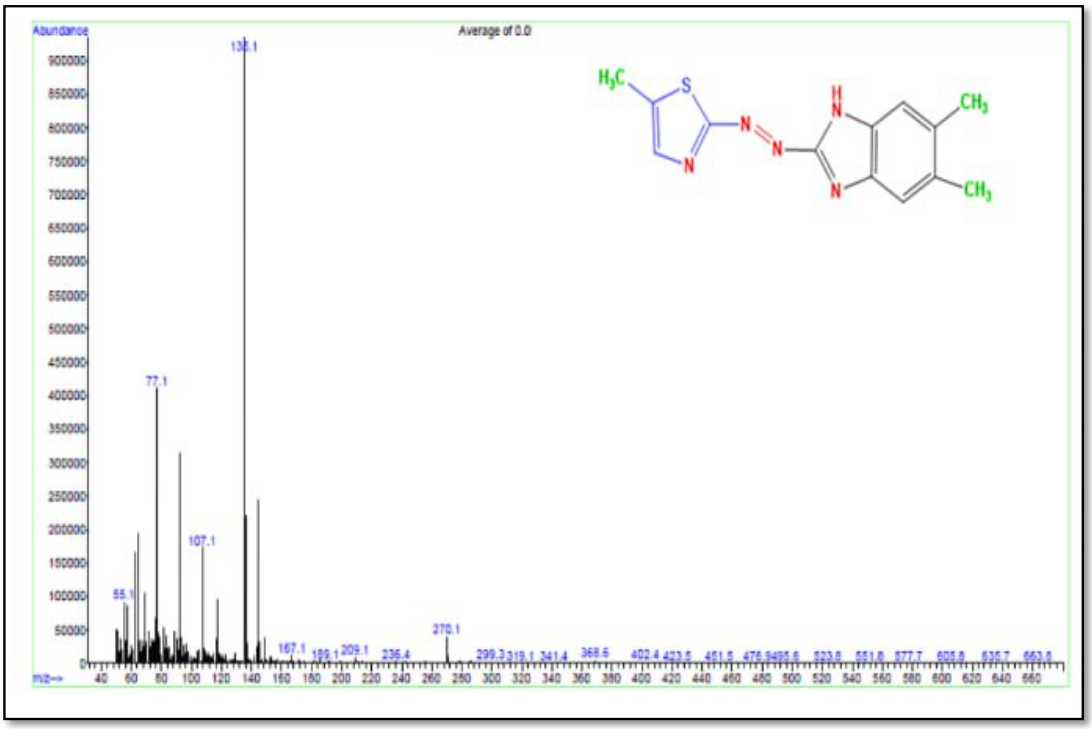

Fig. 11. Mass spectrum for (5-MeTADMBI) ligand.

and (175.17°C -496.19°C) [50].

Mass Spectral Studies

The determination of the molecular weight of the synthesized azo dye is accomplished through the utilization of mass spectrometry, a powerful analytical technique that yields valuable insights into the abundance of ions at various m/z values. Mass spectrometry is a powerful analytical technique that enables the direct identification of molecules by evaluating their mass-to-charge ratio [51].

The thiazolyl azo ligand's mass spectrum revealed a group of peaks, and the compound's predicted mass fractions are illustrated in Figs. 11 and 12. The molecular weight of this compound is 271.34, and the primary peak in the spectral line appeared at (m/z^+= 270.1), which is consistent with the chemical formula [$C_{13}H_{13}N_5S$] Fig. 11.

While the Ni(II)-complex mass spectrum showed a group of peaks and the proposed mass fractions of the Ni(II)-complex was shown in Fig. 12, respectively, the spectrum showed a main peak at (m/z^+= 421.1) that corresponds to the chemical

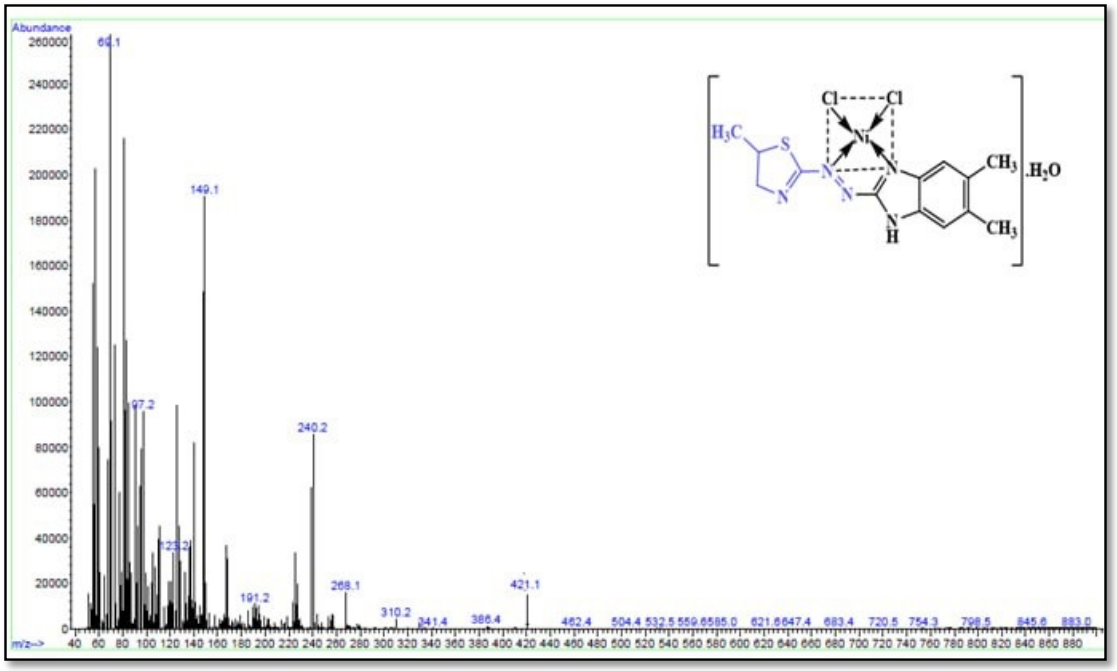

Fig. 12. Mass spectrum for Ni(II) complex

Table 8. Information on the antibacterial activity and inhibition zones of (5-MTADMBI) ligand and its complexes

Compound	Bacteria			Fungi
	Gram-Positive	Gram-Negative		*Candida*
	Streptococcus aureus	*Escherichia coli*	*Klebsiella*	
5-MTADMBI = LH	+++	-	+++	-
$[Co(L)_2Cl_2]Cl.H_2O$	+++	-	+++	-
$[Ni(L)_1Cl_2].H_2O$	++++	-	++++	-
$[Cu(L)_2Cl_2].H_2O$	-	-	++++	-

Highly active = + + ++ (inhibition zone > 30 mm)
Highly active = + + + (inhibition zone > 20 mm)
Moderately active = + + (inhibition zone 15-20 mm)
Weakly active = + (inhibition zone 10-15 mm)
Inactive = - (inhibition zone < 10 mm)

formula [$C_{13}H_{15}N_5SOCl_2Ni$] and belongs to the molecular weight of the compound (418.962) [52].

Anti-microbial activity studies

Antibacterial and antifungal activity

The anti- microbial assay was screened for (5-MTADMBI) ligand and their metal complexes in vitro against bacteria gram-positive, gram-negative (*Staphylococcus aureus, Escherichia coli* and *Klebsiella*) and fungi (*Candida*), using the method of diffusion on Mueller-Hinton agar medium. There was control of the growth-inhibiting zone surrounding the disc. The compounds were dissolved in DMSO to prepare the stock solution. The Petri dishes were subjected to incubation at a temperature of 37 °C for a duration of 24 hours,

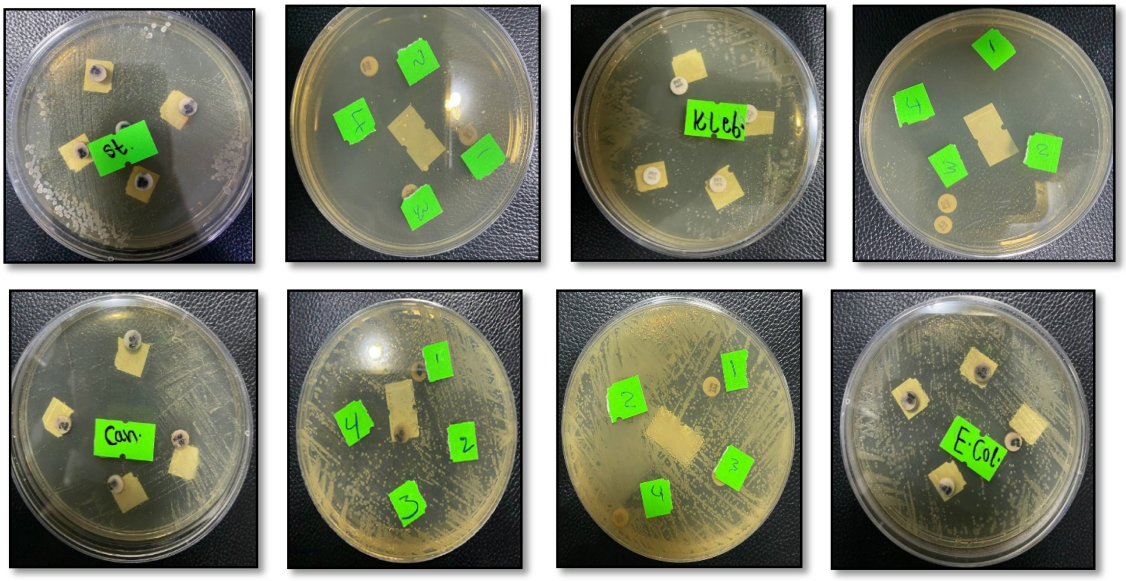

Fig. 13. The inhibition zone for (5-MTADMBI) and its complexes with three types of bacteria and one type of fungi

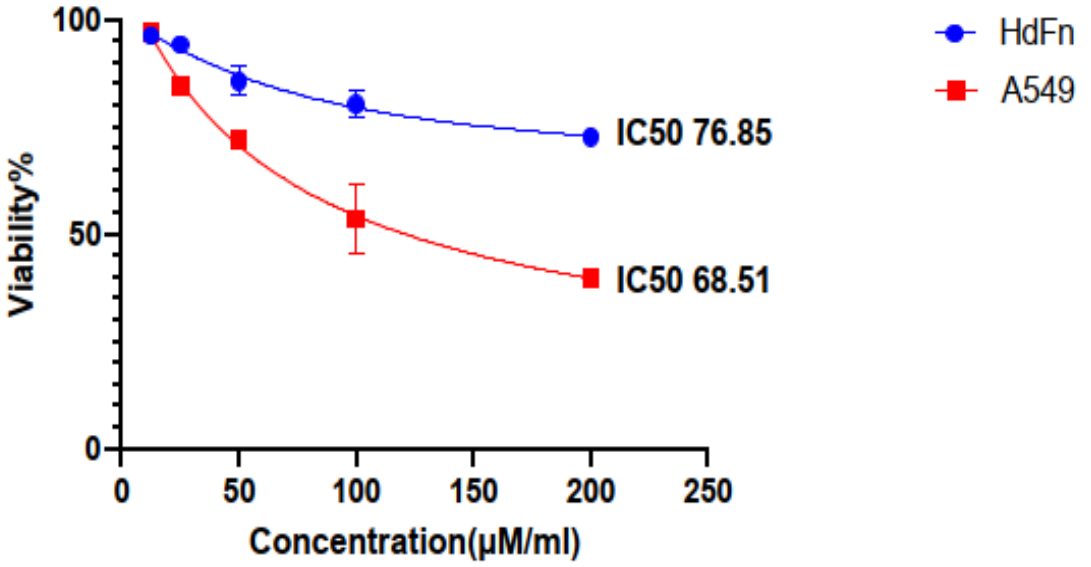

Fig. 14. (5-MTADMBI) ligand IC_{50} (µg/ml) values for cancer cell lines and a normal cell line.

during which the majority of the conducted assays indicate that the complexes exhibit enhanced biological activity in comparison to analogous azo ligands [53,54]. The results are observed in Table 8 and Fig. 13.

Cytotoxicity Assays (MTT assay)

The MTT cell viability assay was employed to quantitatively assess the cytotoxic effects of the azo dye ligand and several metal complexes. The MTT test is commonly used to determine cell viability and calculate the IC50 (half maximal inhibitory concentration) of agents. The MTT assay is a rapid and easy in vitro method for assessing cell viability by measuring the amount of yellow tetrazolium salt reduced to purple formazan [55].

The cytotoxicity of (5-MTADMBI) was assessed by employing the MTT assay within 96-well plates. A confluent monolayer was attained by inoculating cell lines at a density of 1×104 cells per well and allowing them to adhere within a controlled environment of 5% CO_2 incubator for a duration of 24 hours. The experimental setup involved the utilization of DMSO at a concentration of 0.5% (v/v) as the vehicle control for the cultured cells. The negative control, on the other hand, consisted of untreated cells.

The cells were subsequently exposed to several concentrations of (5-MTADMBI) for 48 hours (200, 100, 50, 25, and 12.5 µg/ml). The medium was

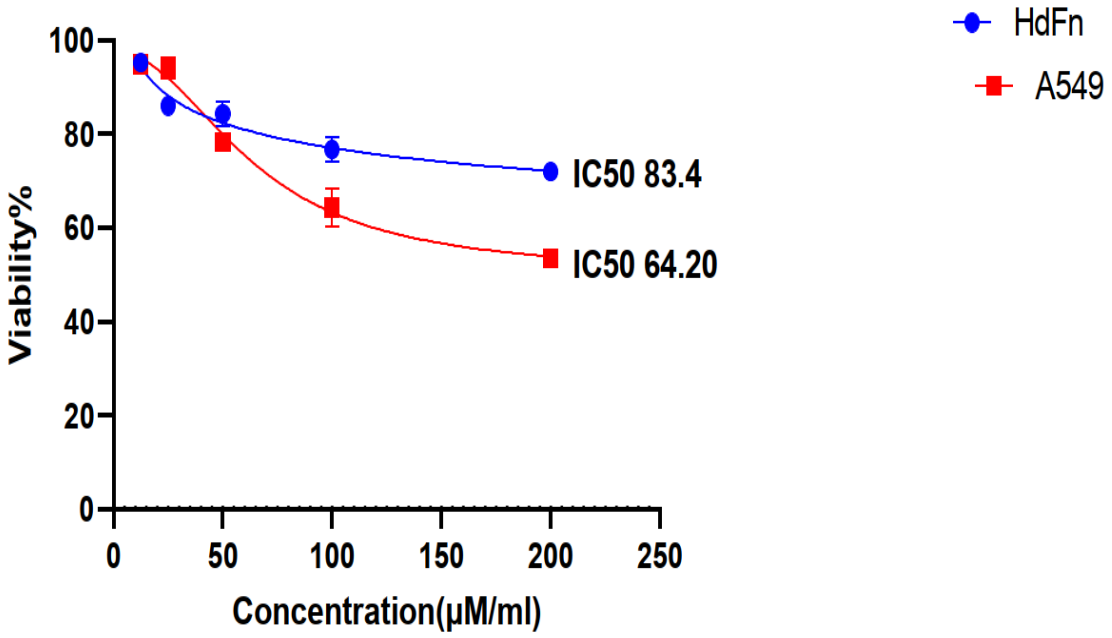

Fig. 15. Cu(II)- complex IC_{50} (µg/ml) values for cancer cell lines and a normal cell line.

Tables 9. Cytotoxicity effect of (5-MTADMBI) ligand on (A459) cells compared with the nature cells lines (HdFn).

Concentration (µg/ml)	LH =5-MTADMBI			
	Cancer line cells		Normal line cells	
	A459		HdFn	
	Cell Viability Mean± SD	% Cell Inhibition	Cell Viability Mean± SD	% Cell Inhibition
200	53.472±1.13	46.528	71.95±0.81	28.05
100	64.39±4.02	35.61	76.69±2.60	23.31
50	78.395±0.75	21.605	84.33±2.66	15.67
25	94.09±2.20	5.91	86.07±1.91	13.93
12.5	94.869±1.39	5.131	95.216±0.82	4.784
IC_{50}	68.51		76.85	

Tables 10. Cytotoxicity effect of Cu-Complex on (A459) cells compared with the nature cells lines (HdFn).

Concentration (µg/ml)	Cu-Complex			
	Cancer line cells		Normal line cells	
	A459		HdFn	
	Cell Viability Mean± SD	% Cell Inhibition	Cell Viability Mean± SD	% Cell Inhibition
200	39.892±2.05	60.108	72.64±1.95	27.36
100	53.43±7.95	46.5	80.20±3.1	19.8
50	71.87±0.46	28.1	85.64±3.32	14.36
25	84.49±0.6	15.51	94.17±0.77	5.83
12.5	96.95±1.23	3.05	96.18±0.23	3.82
IC_{50}	64.20		83.4	

then discarded, and a 5 mg/ml MTT solution was added to each well, where it remained for another 2 to 4 hours at 37 degrees Celsius. Following the successful formation of formazan, DMSO was introduced into the system. Subsequently, the absorbance at a wavelength of 595 nm was meticulously quantified utilizing the cutting-edge technology of an ELISA microplate reader, specifically the xMark Microplate Reader [55].

At 200 (µg.ml $^{-1}$) of the thiazolyl azo ligand, lung cancer (A549) was inhibited at a rate of 60.10%, whereas normal cells (HdFn) were inhibited at a rate of 27.36%. In contrast, the Cu(II)-complex inhibited A549 cells at a rate of 46.528 % at a concentration of 200 (µg.ml −1) and HdFn cells at a rate of 28.05 % at the same dose.

The experimental findings presented in Tables 9 and 10 elucidate the impact of the thiazolyl azo ligand and its Cu(II)-complex on pulmonary cells, while concurrently providing a comparative analysis with the normal cell line at equivalent concentrations. The IC_{50} values, representing the concentration at which 50% inhibition occurs, were determined for lung cancer cells and yielded values of 68.51 and 64.20 (µg.ml^{-1}), respectively. The observed selective cytotoxicity of the ligand and Cu(II)-complex was demonstrated against normal cell lines, with IC_{50} values of 76.85 and 83.4 (µg.ml^{-1}), respectively. Figs. 14 and 15 depict the cell viability percentages of the (5-MTADMBI) ligand and its corresponding Cu(II)-complex, respectively.

CONCLUSION

A predictable diazonium coupling process at 0-5 °C has been used to synthesize a biologically active azo dye ligand, including 5-MeTADMBI Co(III), Cu(II), and Ni(II) were used for metallization with the synthesized azo dye ligand in 1:2 or 1:1 stoichiometric ratio as ligand: metal with the present base. Molar conductivity, elemental analysis, TGA/DTA, Mass, XRD, FE-SEM, FTIR, and nuclear magnetic resonance (NMR) all contributed to the establishment of the structure. The octahedral geometry of the Co(III) and Cu(II) complexes', but square planar for Ni(II) complex, are supported by physicochemical and spectroscopic data. Biological assays showed that both the ligand and its complexes were effective in inhibiting pathogenic bacteria. In addition, each chemical compound gives effective inhibition against the A549 cell line, especially $[Cu(L)_2Cl_2]$. H_2O is considerably more efficient, with IC_{50} values of 64.20.

CONFLICT OF INTEREST

The authors declare that there is no conflict of interests regarding the publication of this manuscript.

REFERENCES

1. Benkhaya S, M'Rabet S, El Harfi A. Classifications, properties, recent synthesis and applications of azo dyes. Heliyon. 2020;6(1):e03271.
2. Heragy MO, Moustafa AAM, Elzanfaly ES, Al-Shareef WA, Saad AS. Miniaturized solid-state sensor for inline monitoring of the microbial biodegradation of a biohazardous textile azo dye (Direct Red-81). Talanta Open. 2022;6:100146.
3. Ahmed R, Khan NA. A short review and study on antimicrobial activity of Unani drug - Ushba (Smilax ornata). Journal of Drug Delivery and Therapeutics. 2019;9(1-s):347-350.
4. Golestaneh Z, Ghashang M. New strategy for the preparation of imidazole derivatives containing thiazole ring via ring opening/coupling/cyclization/decarboxylation cascade. Tetrahedron Lett. 2019;60(44):151194.
5. Al-Adilee KJ, Abedalrazaq KA, Al-Hamdiny ZM. Synthesis and Spectroscopic Properties of Some Transition Metal

Complexes with New Azo-Dyes Derived From Thiazole and Imidazole. Asian J Chem. 2013;25(18):10475-10481.
6. Alves JEF, de Oliveira JF, de Lima Souza TRC, de Moura RO, de Carvalho Júnior LB, Alves de Lima MdC, de Almeida SMV. Novel indole-thiazole and indole-thiazolidinone derivatives as DNA groove binders. Int J Biol Macromol. 2021;170:622-635.
7. Akhileshwari P, Kiran KR, Sridhar MA, Sadashiva MP, Lokanath NK. Synthesis, crystal structure characterization, Hirshfeld surface analysis, and Quantum chemical computations of Ethyl 5-(thiophene-2-carbonyl)thiazole-4-carboxylate. Journal of Molecular Structure. 2021;1242:130747.
8. abdelhamid a, Abd El-Azim M, assy m, Farid W. Heterocyclization of Thiourea Derivative to Novel Azines and Azoles: Antioxidant and Antimicrobial studies. Egyptian Journal of Chemistry. 2022;0(0):0-0.
9. Rizk HF, El-Borai MA, Ragab A, Ibrahim SA, Sadek ME. A Novel of Azo-Thiazole Moiety Alternative for Benzidine-Based Pigments: Design, Synthesis, Characterization, Biological Evaluation, and Molecular Docking Study. Polycyclic Aromatic Compounds. 2021;43(1):500-522.
10. Bera P, Aher A, Brandao P, Manna SK, Bhattacharyya I, Pramanik C, et al. Synthesis, structure elucidation and dft study of a new thiazole–pyridine anchored nnn donor and it's cobalt(II) complex: In-vitro antitumor activity against U937 cancer cells, dna binding property and molecular docking study. Journal of Molecular Structure. 2021;1224:129015.
11. Fathy U, Yousif M, Mohi El-Deen E, Fayed E. Design, Synthesis, and biological evaluation of a novel series of thiazole derivatives based on pyrazoline as anticancer agents. Egyptian Journal of Chemistry. 2022;0(0):0-0.
12. sdeek g, Mauf R, Saleh M. Synthesis and Identification of some new Derivatives Oxazole, Thiazole and Imidazol from Acetyl Cysteine. Egyptian Journal of Chemistry. 2021;0(0):0-0.
13. Zhang D, Ramachandran G, Mothana RA, Siddiqui NA, Ullah R, Almarfadi OM, et al. Biosynthesized silver nanoparticles using Caulerpa taxifolia against A549 lung cancer cell line through cytotoxicity effect/morphological damage. Saudi J Biol Sci. 2020;27(12):3421-3427.
14. Waheeb AS. Spectroscopic, characterization and bioactivity studies of new Ni (II), Cu (II) and Ag (I) complexes with didentate (N,N) donar azo dye ligand. Journal of Molecular Structure. 2023;1276:134729.
15. Waheeb AS, Al-Adilee KJ. Synthesis, characterization and antimicrobial activity studies of new heterocyclic azo dye derived from 2-amino- 4,5- dimethyl thiazole with some metal ions. Materials Today: Proceedings. 2021;42:2150-2163.
16. Kyhoiesh HAK, Al-Adilee KJ. Pt(IV) and Au(III) complexes with tridentate-benzothiazole based ligand: synthesis, characterization, biological applications (antibacterial, antifungal, antioxidant, anticancer and molecular docking) and DFT calculation. Inorg Chim Acta. 2023;555:121598.
17. Kyhoiesh HAK, Al-Adilee KJ. Synthesis, spectral characterization and biological activities of Ag(I), Pt(IV) and Au(III) complexes with novel azo dye ligand (N, N, O) derived from 2-amino-6-methoxy benzothiazole. Chemical Papers. 2022;76(5):2777-2810.
18. Al-Adilee K, Kyhoiesh HAK. Preparation and identification of some metal complexes with new heterocyclic azo dye ligand 2-[2 – - (1- Hydroxy -4- Chloro phenyl) azo]- imidazole and their spectral and thermal studies. Journal of Molecular Structure. 2017;1137:160-178.
19. Al-Adilee KJ, Atyha SA. Synthesis, Spectral, Thermal and Biological Studies of Some Metal Complexes Derived from Heterocyclic Mono Azo Dye Ligand 2'[(2'-Hydroxy-4-methyl phenyl)azo]imidazole. Asian J Chem. 2018;30(2):280-292.
20. Al-Adilee KJ, Abass AK, Taher AM. Synthesis of some transition metal complexes with new heterocyclic thiazolyl azo dye and their uses as sensitizers in photo reactions. Journal of Molecular Structure. 2016;1108:378-397.
21. Waheeb AS, Kadhim Kyhoiesh HA, Salman AW, Al-Adilee KJ, Kadhim MM. Metal complexes of a new azo ligand 2-[2-(5-nitrothiazolyl) azo]-4-methoxyphenol (NTAMP): Synthesis, spectral characterization, and theoretical calculation. Inorg Chem Commun. 2022;138:109267.
22. Christensson N, Žídek K, Magdaong NCM, LaFountain AM, Frank HA, Zigmantas D. Origin of the Bathochromic Shift of Astaxanthin in Lobster Protein: 2D Electronic Spectroscopy Investigation of β-Crustacyanin. The Journal of Physical Chemistry B. 2013;117(38):11209-11219.
23. Al-Khateeb ZT, Karam FF, Al-Adilee K. Synthesis and characterization of some metals complexes with new heterocyclic azo dye ligand 2-[2- (5- Nitro thiazolyl) azo]-4-methyl -5- nitro phenol and their biological activities. Journal of Physics: Conference Series. 2019;1294(5):052043.
24. Abd ZZ, Abbas AK. Metal Complexes of Adenine Azo Ligand: Synthesis, Identification and Study some of their Applications. Iraqi Journal of Science. 2024:1212-1229.
25. Hameed G, Wadday F, Farhan M, Hussain S. Synthesis, Spectroscopic characterization and bactericidal valuation of some metal (II) complexes with new Tridentate Heterocyclic Azo Ligand Type (NNO) Donor. Egyptian Journal of Chemistry. 2020;0(0):0-0.
26. Teixeira EI, Schwalm CS, Casagrande GA, Tirloni B, Schwade VD. Binuclear isophthaloylbis(N,N-diphenylthioureate) transition metal complexes: Synthesis, spectroscopic, thermal and structural characterization. Journal of Molecular Structure. 2020;1210:127999.
27. Yallur BC, Krishna PM, Challa M. Bivalent Ni(II), Co(II) and Cu(II) complexes of [(E)-[(2-methyl-1,3-thiazol-5-yl)methylidene]amino]thiourea: synthesis, spectral characterization, DNA and in-vitro anti-bacterial studies. Heliyon. 2021;7(4):e06838.
28. J. Al-Adilee K, Adnan S. Synthesis and Spectral Properties Studies of Novel Hetrocyclic Mono Azo dye Derived from Thiazole and Pyridine with Some Transition Complexes. Oriental Journal of Chemistry. 2017;33(04):1815-1827.
29. Shaker SA. Preparation and Study of Some Mn(II), Co(II), Ni(II), Cu(II), Cd(II) and Pb(II) Complexes Containing Heterocyclic Nitrogen Donor Ligands. E-Journal of Chemistry. 2010;7(4):1598-1604.
30. Al-Saffar ZH, Yaacob H, Al Jawahery MS, Yousif ST, Satar MKIM, Jaya RP, et al. Extraction and Characterisation of Maltene from Virgin Asphalt as a Potential Rejuvenating Agent. Sustainability. 2023;15(2):909.
31. Safaei-Farouji M, Jafari M, Semnani A, Gentzis T, Liu B, Liu K, et al. TGA and elemental analysis of type II kerogen from the Bakken supported by HRTEM. Journal of Natural Gas Science and Engineering. 2022;103:104606.
32. Niluvanji Matada M, Jathi K, Rangappa MM, Geoffry K, Ravi Kumar S, Nagarajappa RB, Noor Zahara F. A new sulphur containing heterocycles having azo linkage: Synthesis, structural characterization and biological evaluation.

Journal of King Saud University - Science. 2020;32(8):3313-3320.
33. Al-Adilee KJ, Jawad SH, Kyhoiesh HAK, Hassan HM. Synthesis, characterization, biological applications, and molecular docking studies of some transition metal complexes with azo dye ligand derived from 5-methyl imidazole. Journal of Molecular Structure. 2024;1295:136695.
34. Abbas BF, Abdulla ZS, Abid Al-jibouri MN. Preparation and Spectroscopic Studies of Some Metal complexes with Azo ligand derived from 2-aminobenzothiazole and 4-Hydroxycoumarin. Research Journal of Chemistry and Environment. 2022;26(10):164-171.
35. Lyčka A. Multinuclear NMR of azo dyes and their metal complexes. Annual Reports on NMR Spectroscopy: Elsevier; 2000. p. 1-57.
36. Abu-Dief AM, El-Metwaly NM, Alzahrani SO, Alkhatib F, Abualnaja MM, El-Dabea T, El-Remaily MAEAAA. Synthesis and characterization of Fe(III), Pd(II) and Cu(II)-thiazole complexes; DFT, pharmacophore modeling, in-vitro assay and DNA binding studies. J Mol Liq. 2021;326:115277.
37. Kyhoiesh HAK, Al-Adilee KJ. Synthesis, spectral characterization, antimicrobial evaluation studies and cytotoxic activity of some transition metal complexes with tridentate (N,N,O) donor azo dye ligand. Results in Chemistry. 2021;3:100245.
38. Bourouina A, Rekis M. Comparison in optoelectronic properties of triphenylamine-imidazole or imidazole as donor for dye-sensitized solar cell: theoretical approach. J Mol Model. 2021;27(8).
39. shahzad k, Abbas F, Pandey D, Ajmal S, Khadim M, tahir Mu. Synthesis, Characterization and Biological Evaluation of Novel Tetrasubsituted Imidazole Compounds. American Chemical Society (ACS); 2020.
40. K. Ahmed A, K. Jebur I, Ali Muayad Hamzah M. Synthesis, Characterization and Biological Activity Evaluation of Some New Azo Derivatives from 2- Amino Benzothiazole and Their Derivatives. Kirkuk University Journal-Scientific Studies. 2018;13(1):212-227.
41. Abdulrazzaq AG, Al-Hamdani AAS. Cr (III), Fe (III), Co (II) and Cu(II)Metal ions complexes with azo compound derived from 2-hydroxy quinolin synthesis, characterization, thermal study and antioxidant activity. Ibn AL-Haitham Journal For Pure and Applied Sciences. 2023;36(3):214-230.
42. NVEO - NATURAL VOLATILES and ESSENTIAL OILS Journal | NVEO.
43. Stanjek H, Häusler W. Basics of X-ray Diffraction. Hyperfine Interactions. 2004;154(1-4):107-119.
44. Ortiz C, Vega F, Solis J. Particulates in laser-deposited copper oxide films. Thin Solid Films. 1992;218(1-2):182-186.
45. Holzwarth U, Gibson N. The Scherrer equation versus the 'Debye-Scherrer equation'. Nature Nanotechnology. 2011;6(9):534-534.
46. Tyuftin AA, Mohammed H, P. Kerry J, O'Sullivan MG, Hamill R, Kilcawley K. Microscopy-Assisted Digital Photography as an Economical Analytical Tool for Assessment of Food Particles and Their Distribution Through The use of the ImageJ Program. Advances in Nutrition and Food science. 2021;2021(02).
47. Shakir M, Hanif S, Sherwani MA, Mohammad O, Al-Resayes SI. Pharmacologically significant complexes of Mn(II), Co(II), Ni(II), Cu(II) and Zn(II) of novel Schiff base ligand, (E)-N-(furan-2-yl methylene) quinolin-8-amine: Synthesis, spectral, XRD, SEM, antimicrobial, antioxidant and in vitro cytotoxic studies. Journal of Molecular Structure. 2015;1092:143-159.
48. Kusmariya BS, Tiwari S, Tiwari A, Mishra AP, Naikoo GA, Pandit UJ. Theoretical and experimental studies of two Co(II) and Ni(II) coordination complex with N,O donor 2-chloro-6-{[(4-hydroxy-3-methoxyphenyl)methylidene] amino}-4 nitrophenol ligand. Journal of Molecular Structure. 2016;1116:279-291.
49. Alaghaz A-NMA, Al-Sehemi AG, El-Gogary TM. Synthesis, characterization and quantum chemical ab initio calculations of new dimeric aminocyclodiphosph(V)azane and its Co(II), Ni(II) and Cu(II) complexes. Spectrochimica Acta Part A: Molecular and Biomolecular Spectroscopy. 2012;95:414-422.
50. Khanum R, Shoukat Ali RA, Rangaswamy HR, Santhosh Kumar SR, Prashantha AG, Jagadisha AS. Recent review on Synthesis, spectral Studies, versatile applications of azo dyes and its metal complexes. Results in Chemistry. 2023;5:100890.
51. Harisha S, Keshavayya J, Kumara Swamy BE, Viswanath CC. Synthesis, characterization and electrochemical studies of azo dyes derived from barbituric acid. Dyes and Pigments. 2017;136:742-753.
52. Alshater H, Al-Sulami AI, Aly SA, Abdalla EM, Sakr MA, Hassan SS. Antitumor and Antibacterial Activity of Ni(II), Cu(II), Ag(I), and Hg(II) Complexes with Ligand Derived from Thiosemicarbazones: Characterization and Theoretical Studies. Molecules. 2023;28(6):2590.
53. Sharma B, Shukla S, Rattan R, Fatima M, Goel M, Bhat M, et al. Antimicrobial Agents Based on Metal Complexes: Present Situation and Future Prospects. International Journal of Biomaterials. 2022;2022:1-21.
54. Basim S, Kasim A. Cytotoxic Activity of the Ethyl Acetate Extract of Iraqi Carica papaya Leaves in Breast and Lung Cancer Cell Lines. Asian Pac J Cancer Prev. 2023;24(2):581-586.
55. Ahmed OH, Bdulqader AA, Ezghayer MA. Antibacterial activity of methanolic extract of leaves Indigofera Suffruticosa naturally grown in Iraq. Journal of Advanced Pharmacy Education and Research. 2023;13(4):99-103.